

Relations between Annular Modes and the Mean

State:

Southern Hemisphere Winter.

FRANCIS CODRON *

Laboratoire de Météorologie Dynamique, Université Pierre et Marie Curie-Paris6 / CNRS, Paris, France

Submitted to Journal of Atmospheric Sciences

October 23, 2006

**corresponding author address:* Dr. Francis Codron, Laboratoire de Météorologie Dynamique, Université Pierre et Marie Curie-Paris6, 75005 Paris, France.
Email: fcodron@lmd.jussieu.fr

ABSTRACT

In a zonally-symmetric climatology with a single eddy-driven jet, such as prevails in the Southern Hemisphere summer, the mid-latitude variability is dominated by fluctuations of the jet around its mean position, as described by the Southern Annular Mode (SAM). To study whether this result holds for a zonally asymmetric climatology, the observed variability of the Southern Hemisphere winter is analyzed. The mean state in this case is characterized by relatively weak stationary waves; yet there exist significant zonal variations in the mean strength and meridional structure of the subtropical jet stream.

As in summer, the winter SAM signature is annular in shape and the corresponding wind anomalies are dipolar; but it is associated with two different behaviors of the eddy-driven jet in different longitudinal ranges. Over the Indian Ocean, the SAM is associated primarily with a latitudinal shift of the jet around its mean position. Over the Pacific sector, it is instead characterized by a see-saw in the wind speed between two distinct latitudes, corresponding to the positions of the midlatitude and subtropical jets. Composites of eddy-forcing and baroclinicity over both sectors appear consistent with the two different behaviors.

As in the zonal-mean case, high-frequency eddies both force and maintain the low-frequency wind anomalies associated with the SAM. The positive feedback by eddies is however not local: changes in the eddy-forcing are influenced most strongly by zonal wind anomalies located upstream.

1. Introduction

Quasi-annular patterns, often called annular modes, dominate atmospheric extra-tropical low-frequency variability (Thompson and Wallace 1998). For both hemispheres, these modes are characterized by pressure anomalies of one sign over the polar region, surrounded by a band of opposing polarity with peak amplitude in the midlatitudes. They also appear as the favored response to a wide range of climate forcings, such as: the observed trend in the Southern Hemisphere (Thompson and Solomon 2002), the observed Southern Hemisphere response to El Niño (Seager et al. 2003; L'Heureux and Thompson 2006), as well as the modeled response to greenhouse gas increase (Kushner et al. 2001) or ozone depletion (Gillett and Thompson 2003; Arblaster and Meehl 2006).

From the physical point of view, annular modes have been studied in association with the dynamics of zonally-averaged wind fluctuations. The variability of a zonal eddy-driven jet is dominated by a dipolar, equivalent-barotropic zonal wind anomaly centered on the jet core, in models (Robinson 1996, 2000) as well as in observations (Lorenz and Hartmann 2001; Feldstein and Lee 1998). This structure is sustained by a positive feedback from high-frequency eddies.

Based on these results, it has been suggested that annular modes could arise from such zonally-symmetric dynamics, each time modified by local characteristics, such as position and strength of storm tracks or baroclinic zones (Cash et al. 2005). Quadrelli and Wallace (2002) showed, for example, that the northern annular mode structure changes with the phase of El Niño. It is not clear, however, to what degree of zonal asymmetry this paradigm holds. Ambaum et al. (2001) argue, for example, that the Northern Hemisphere variability is best described using different regional patterns.

To study annular modes in progressively less zonally-symmetric climatologies, this paper extends and completes the study of Codron (2005). The two papers together explore the transition from pure zonal-mean dynamics to quasi-annular patterns in a zonally-varying basic state, by analyzing the annular mode in increasingly complex climatologies, constructed from different seasons or phases of El Niño. The focus is on the variation of the structure and the amplitude of the annular

mode, as well as on the extent to which the dynamics of the zonally-averaged case apply in the presence of zonal asymmetries.

[Figure 1 about here.]

The Southern Hemisphere midlatitudes are characterized by weak stationary waves. The climatological 300-hPa zonal wind for the months of Dec-Jan, Mar-Apr and Jun-Jul-Aug is shown in Fig. 1. In summer and fall there is only one eddy-driven jet, mostly zonally-symmetric (although a weak subtropical jet appears in fall). In a previous paper (Codron 2005), it was shown that in these two seasons the SAM consists, at all longitudes, in a dipole of wind anomalies centered on the jet maximum. Between different climatologies, the annular mode follows the latitudinal variations of the mean jet, albeit with differences in variance. Consistently with theory, the SAM wind anomalies are reinforced by eddy-feedback. In winter, the situation is complicated by the additional presence of a strong subtropical jet over the Indian and Pacific oceans. The subtropical and midlatitude jet strengths peak at different longitudes, so that a wide range of behaviors is possible. An analysis of the origins of the winter zonal asymmetries can be found for example in Inatsu and Hoskins (2004).

The Southern Hemisphere winter is the focus of this paper, that develops as follows: section 2 describes the data and analysis procedures used. The winter SAM structure is analyzed in section 3: section 3a compares the large-scale pattern with the summer and fall cases; then section 3b shows in more detail the different relations of the SAM with the climatological-mean structures at different longitudes. Section 4 discusses the dynamics of the SAM, while section 5 tests the robustness of the results. The main findings are summarized in section 6.

2. Analysis procedures

a. Data

The observations used in this study are based on the NCEP-NCAR reanalysis data set (Kalnay and Coauthors 1996), from 1958 through 2001, on a $2.5^\circ \times 2.5^\circ$ grid. To define the different

seasonal-mean states, subsets of the monthly data are created by considering December-January (DJ), March-April (MA) and June-July-August (JJA) separately. The two- and three-calendar month subsets are 88 and 132-month long, respectively. Before the principal component analysis, a trend equal to the best cubic fit was removed at each point. The analyses were repeated with removal of a linear trend or of only the seasonal cycle, without affecting the results. For daily fields, a daily seasonal cycle and trend, computed after applying a 30-day running mean, are removed from the original data.

Since the reanalysis data are not fully reliable in the Southern Hemisphere before 1979, our analyses were repeated for the subset of the data extending from 1979 onward, and no significant differences were found.

b. Methods

1. SOUTHERN ANNULAR MODE

The Southern Annular Mode (SAM) is defined as the first principal component of Southern Hemisphere monthly 850-hPa geopotential height anomalies (poleward of 20°S), after the data were weighted by the square-root of the cosine of latitude to account for the change of area with latitude.

SAM-related anomaly patterns for several fields are obtained by a linear regression upon the standardized monthly SAM time series; while SAM composites are constructed by averaging over months when the SAM time series is higher (or lower) than plus (or minus) one and a half standard deviation. By convention, the positive phase corresponds to negative pressure anomalies over the South Pole.

For lagged-correlation computations, a daily SAM time series is obtained by projecting the daily 850-hPa geopotential field upon the spatial pattern obtained by regression onto the monthly SAM time series.

2. EDDY FORCING

The forcing of the zonal flow by high-frequency eddies at 300-hPa is based on daily values of the wind speed, separated into high and low frequency components using the filter described in Blackmon and Lau (1980), with a 10-day period cutoff. The eddy momentum flux convergence, or eddy forcing (EF), is computed as $\frac{1}{a \cos^2 \phi} \partial_{\phi}(u^* v^* \cos^2 \phi)$, where ϕ is latitude, a is the radius of the Earth, and the star denotes the wind departure from its zonal mean.

Daily time series of the EF of the SAM were constructed by projecting the zonal-mean EF on the latitudinal structure of the SAM 300-hPa zonal wind anomalies.

3. Description of the SAM structure

a. Hemispheric analysis

[Figure 2 about here.]

The regressions of the 850-hPa geopotential height onto the SAM time series are shown on the top panels of Fig. 2 for the three different climatologies of Fig. 1: DJ, MA and JJA. The structure is roughly annular in all cases. The SAM is generally well separated from the second EOF, the respective variance explained of 27% and 14% for JJA being typical. The covarying upper tropospheric wind fields are shown in the lower panels of Fig. 2 for the 300-hPa level, where the eddy-driven jet and the zonal index wind anomaly are strongest (Lorenz and Hartmann 2001).

For the summer subsets, DJ and MA, the strong correspondence between the node of the SAM signature and the maximum of the climatological jet (shown again as a continuous black line) indicates that at all longitudes the SAM represents (to first order) a latitudinal shift of the jet. The positive SAM phase is associated with a poleward displacement of the eddy-driven jet, and vice-versa. This relationship holds for both subsets, even though the climatological jet is farther equatorward in DJ than in MA (Codron 2005).

The winter subset, JJA, exhibits a very different behavior, as shown in the right panels of Fig. 2. As for the summer subsets, the location of the SAM node over the Indian ocean corresponds to the

maximum of the midlatitude jet. However, over the western Pacific the location of the SAM node corresponds to the line of *minimum* zonal wind speed (shown as a dashed black line) between the subtropical and midlatitude jets. In this case, the maximum climatological wind speeds are aligned with maximum SAM anomalies of either sign: positive SAM anomalies for the midlatitude jet and negative SAM anomalies for the subtropical jet. Therefore, it appears that in the Pacific sector, for JJA, the SAM represents more an out-of-phase strengthening/weakening of the two jets, rather than the usual midlatitude jet shift.

The peculiar behavior of the wintertime SAM over the Pacific sector is evident when comparing composites of the 300-hPa zonal wind for the two phases (Fig. 3). In the positive SAM phase, a clear midlatitude jet appears over the Pacific ocean, well separated from the subtropical jet. In the negative SAM phase, the midlatitude jet is absent and the subtropical jet is stronger. Over the Indian ocean, the midlatitude jet is visible in both phases and it just shifts poleward in the positive SAM polarity, as is more typically observed.

[Figure 3 about here.]

To study in more detail the two different SAM behaviors in JJA, further analyses are carried on separately for two adjacent 90°-longitude sectors, referred to as the "Indian" (30-120°E) and "Pacific" (120-210°E) sectors. The boundary between the two sectors, at 120°E (indicated in Fig. 3 by a dashed line), represents the range of longitudes where the relationship between the SAM and the mean wind changes, as seen in Fig. 2.

b. JJA: Sectoral analysis

SAM composites of several fields, zonally-averaged over the Indian and Pacific sectors, respectively, are shown in Fig. 4 for JJA. At the 300-hPa level, where the flow is dominated by the presence of the subtropical jet, both sectors are characterized by a double-jet structure. The relative intensity of the two jets varies between the opposing polarities of the SAM. In the positive SAM composite, the midlatitude jet is stronger and the subtropical jet is slightly weaker than in

the negative SAM composite. Over the Pacific sector the midlatitude jet exhibits a much stronger relative change in speed between the opposing SAM polarities, and does not show the latitudinal shift observed over the Indian sector.

[Figure 4 about here.]

At lower levels, the Hadley cell-driven subtropical jet becomes less important, and the observed westerly winds are due to the forcing by eddies. Therefore, given that the SAM dynamics involve interactions between wind and baroclinic eddies, the SAM signature will be clearest at such lower levels, for example 850-hPa.

Indeed, in the Indian sector the 850-hPa zonal wind is close to zero directly beneath the subtropical jet maximum, for both polarities of the SAM. The single eddy-driven jet, located farther south, simply shifts latitudinally between the two SAM polarities, being poleward (and slightly stronger) in the positive polarity.

At the same level in the Pacific sector, the meridional structure of the wind exhibits a more complex behavior. In the negative polarity of the SAM, the eddy-driven jet encompasses a wide latitudinal range. Two distinct maxima, equally intense, are observed at the latitudes of the midlatitude jet and of the poleward flank of the subtropical jet. In the positive polarity of the SAM, only the poleward maximum remains; it occurs at the same latitude as in the negative phase, but with a speed about twice as large.

The high-frequency EF composites are consistent with the behavior of the eddy-driven jets described in the previous paragraph. In the Indian sector, the westerly momentum leaving the subtropical jet is deposited slightly poleward of the midlatitude jet, at a latitude that shifts with the phase of the SAM (poleward for the positive polarity of the SAM). In the Pacific sector, westerly momentum is deposited in two distinct regions, that correspond to the maxima in the zonal wind. Neither EF maximum, however, shows a latitudinal shift between the opposite SAM polarities. Rather, it is the relative amplitude of the two EF peaks that reverses, as in a see-saw. For the positive polarity of the SAM the poleward maximum is stronger, and vice-versa.

The previous results taken together define the following overall picture for JJA:

- in the Indian sector, the variability associated with the SAM is, to first order, a barotropic latitude shift of the (single) jet, accompanied by a consistent shift of the eddy forcing. This is the behavior generally observed in other seasons (Codron 2005) and in the zonal-average case;
- in the Pacific sector, two jets, each associated with a well defined storm track, are observed at two distinct latitudes. In this case, the SAM represents a see-saw in the strength of these two jets (and of their storm tracks). This behavior resembles “split jet” variability, as described for example in Yang and Chang (2006), Bals-Elsholz et al. (2001), and Inatsu and Hoskins (2006).

4. Dynamical mechanisms

a. Meridional profile of baroclinicity

The baroclinicity composites shown in Fig. 5 provide some possible insight into the origins of the different behaviors of the SAM in the two sectors. The baroclinicity measure used here ($g \frac{\Theta_y}{\Theta_0 N}$) is proportional to the Eady growth rate at 850-hPa. Generation and growth of baroclinic waves are expected to be stronger in regions of high baroclinicity. When waves propagate away, westerly momentum will converge into these source regions, thus sustaining an eddy-driven jet.

In the Indian sector, a wide zone of high baroclinicity is observed at the latitudes of the eddy-driven jet (40-55°). The maximum baroclinicity shifts within this zone from a poleward to an equatorward location between the positive and negative SAM phases, following the shift of the jet and storm tracks.

In the Pacific sector, the mean baroclinicity is higher in the Tropics and much weaker at mid-latitudes, in comparison to that in the Indian sector. Indeed, two regions of comparably strong baroclinicity are observed at about 30-35° and 55-60°, separated by an area of weak baroclinicity. The latitudes of these two regions correspond to the maxima of the two eddy-forcing regions seen on Fig. 4. In the positive polarity of the SAM, baroclinicity is stronger at high latitudes and weaker

in the Tropics, and the poleward jet dominates. In the negative polarity of the SAM, baroclinicity is almost equal in the two regions, and so is the 850-hPa wind speed.

[Figure 5 about here.]

These observations are consistent with the numerical results obtained by Lee and Kim (2003). Using an idealized primitive equations model and initial-value experiments with varying tropical heating, they showed that the largest generation of baroclinic waves shifted abruptly from mid-latitudes to the poleward flank of the subtropical jet when the latter became strong enough. The threshold was crossed for approximately equal Eady growth rates at the two latitudes. A similar behavior was also observed in equilibrium experiments (Son and Lee 2005), with a smoother transition from a double jet structure with an independent midlatitude jet to a single subtropical jet.

In view of these results, the observed SAM behavior could therefore be tentatively interpreted as follows:

- in the Indian sector, the strong baroclinicity at midlatitudes guarantees the presence of a separate midlatitude jet in addition to the subtropical jet. Moreover, the zone of strong baroclinicity is wide enough to accommodate the latitudinal shifts in the jet location;
- in the Pacific sector, the meridional structure of the baroclinicity, with comparably high values at midlatitudes and in the subtropics, is close to a potential “threshold”. In this situation, a small change in the forcing is able to shift the balance in favor of wave growth in either region.

b. Eddy forcing and feedback

The prominence of annular modes of variability is thought to be a consequence of a positive feedback by high-frequency eddies on low-frequency mean flow anomalies (Robinson 1996; Lorenz and Hartmann 2001). To test this hypothesis, the feedback component must be first separated from the random forcing of the SAM by the eddies themselves. Since positive instantaneous

correlations do not imply a feedback (Feldstein and Lee 1998), a solution is to focus on the forcing by the eddies at lags greater than their own decorrelation timescale, 3 to 5 days.

The relationship between the 300-hPa zonal wind and its forcing by high-frequency eddies (or eddy forcing, EF) is shown in Fig. 6. The lagged cross-correlation with the daily SAM time series is shown for the complete zonal average, and for independent averages over the Indian and Pacific sectors.

[Figure 6 about here.]

The shape of the cross-correlation curve is similar to that found by Lorenz and Hartmann (2001) for the whole year and by Codron (2005) for the summer season. The correlation peak occurs when EF leads by a few days, consistent with the zonal wind being forced by eddies. The small but positive correlation at lags longer than a few days indicates an organization of eddies by the SAM leading to a positive feedback. The magnitude of the correlations at positive lags is comparable to the ones obtained by Lorenz and Hartmann (2001); Codron (2005) or Watterson (this issue) in other configurations. The significance of the correlations was computed by estimating the effective number of degrees of freedom from the auto-correlation of the two time series, as in Bretherton et al. (1999). The eddy feedback is strongest for the total zonal average, but the lagged forcing of SAM wind anomalies is also significant at 95% over the Pacific sector.

The meridional structure of the lagged EF, averaged between lags 5 and 20, is shown in Fig. 7 for high-frequency as well as total EF, together with the SAM wind anomalies. The lagged EF profiles can be considered as the EF response to the SAM wind anomalies. The high-frequency EF has a dipolar shape with a narrower meridional scale than the SAM wind anomalies. In particular, the equatorward lobe is shifted southward compared to the SAM wind anomaly, again reminiscent of the results for the summer season. The (latitude-weighted) pattern correlation between lagged EF and 300-hPa SAM wind anomalies is 0.67. The analogous correlation obtained by using total EF is lower but still positive (0.31).

[Figure 7 about here.]

Similar pictures are obtained for averages of the lagged high-frequency EF over the Indian and Pacific sectors (not shown). The pattern correlations of the SAM wind anomalies with high-frequency EF are 0.40 and 0.57, respectively, for the two sectors.

Using a storm-track model, Yang and Chang (2006) also found an eddy feedback in the Pacific split-jet sector for similarly shaped wind anomalies. The dynamical processes responsible for the zonally-averaged SAM thus seem to apply at least to the Pacific sector, despite the different relations of the SAM anomalies with the climatological jets. Over the Indian sector, there is a strong forcing by eddies but little feedback. The possible reasons for this different behavior are further explored now.

c. Non-local transients organization

Figure 8 shows SAM wind-EF lag-correlations, as in Fig. 6 but for the Pacific sector EF only, with different SAM indices: the daily SAM time-series, as well as the daily 300-hPa SAM wind anomalies independently averaged over the Indian and over the Pacific sectors.

As expected, for eddies leading by a few days (EF forcing the zonal wind), the strongest correlation of the Pacific EF is observed with SAM wind anomalies also averaged over the Pacific sector. However, at positive lags (eddy feedback), the correlation of the Pacific EF is highest with SAM wind anomalies over the Indian sector, and lowest with SAM wind anomalies over the Pacific sector. This result is robust whether or not days outside JJA are used to compute the lagged-correlations, or however the time-series were detrended.

[Figure 8 about here.]

The spatial pattern correlations also show that the EF over the Pacific sector projects best on the local SAM wind structure when lagging SAM wind anomalies averaged over the Indian sector (0.62), and not with those averaged over the Pacific sector. No such relation is found for the Indian EF, which is always weak at all positive lags (not shown).

[Figure 9 about here.]

A possible explanation for the relationship between sectors lies in the fact that most of the kinetic energy of high-frequency eddies is concentrated in zonally-localized (about 120° longitude) traveling wave packets (Chang 2005). The zone where the eddies decay and accelerate the jet is located downstream (eastward) of their zone of growth, where they are organized by local baroclinicity. Thus, the EF over the Pacific is strongly influenced by upstream flow anomalies that occur over the Indian sector. The group velocity of observed wavepackets is close to 26 per day (Chang 2005), yielding a timescale for propagation between the two sectors of 3-4 days, so it is not limiting for the periods considered here.

Another way to see this predominant downstream influence is demonstrated on figure 9, which shows composites of EF over the two sectors lagging positive or negative SAM wind anomalies by 10-25 days. For EF over the Pacific sector lagging the upstream Indian sector wind anomalies, the composites are very similar to those of monthly means (figure 4). In the reverse situation, however, the Indian sector EF composites lagging the Pacific wind anomalies of either SAM polarity are almost undistinguishable. The lack of a Pacific to Indian sector influence means that the reverse signal is not an artefact of spatial autocorrelation, but is due to some mechanism of downstream propagation.

In the Indian sector, which lies downstream of a region of low SAM amplitude, the eddies are not as well organized as in the Pacific, and their feedback on the zonal flow is weaker. The eddy variance, in particular that of the EF of the SAM, is however very high. The high amplitude of the SAM in the Indian sector thus seems due more to a random but strong EF than to a positive feedback; a situation reminiscent of the March-La Niña experiment in Codron (2005).

Therefore, the observed JJA SAM appears to be different from a fully zonally-symmetric situation, in which growth and decay would occur at all longitudes simultaneously. Here instead, the eddy-mediated upstream/downstream relationship provides a possible mechanism for extending zonal wind and geopotential height anomalies in the zonal direction, helping to give the SAM its large spatial scale. Similar mechanisms might also explain the tendency for the extratropical response to slow forcings, such as the ENSO cycle (Seager et al. 2003) or the increase in greenhouse

gases (Arblaster and Meehl 2006; Gillett and Thompson 2003), to assume a zonally-symmetric shape.

5. Robustness of the results.

The SAM, whose index is obtained through a statistical method, does not necessarily represent a favored mode of variability of the physical system. This section discusses two issues concerning the SAM that may possibly arise.

A first argument against the existence of annular modes is the fact that they do not reflect actual correlations of variables over different regions. It has been argued that the midlatitude variability would be better described by an ensemble of longitudinally-localized patterns with the same meridional structure as the SAM (Cash et al. 2005; Ambaum et al. 2001).

To investigate the correlation between the Pacific and Indian sectors, two regional EOFs were independently computed using only height data from each sector. The first EOF in each sector explains 42% and 39% of the local variance (and 19% and 18% for the second EOF). The 850-hPa height patterns, obtained by regressing the global height onto each of the regional PCs, are shown in Fig. 10. Both are very similar to the global SAM signature, with just a small regional emphasis. In particular, the low-pressure anomaly is located over the pole in both cases. The time-series associated with these EOFs are correlated at .78, and each one is correlated with the SAM PC at .90. These correlations between 90-sector EOFs are high, compared for example to the model results of Watterson (this issue).

[Figure 10 about here.]

The bottom panels of Fig. 10 show that the meridional structure of wind anomalies is the same over both sectors, regardless of whether the SAM or either regional EOF is used. As no data outside of their respective sectors were used to compute the regional EOFs, these similarities reflect actual correlation between the SAM structures in the two sectors.

A second argument, analogue to that of Ambaum et al. (2001) for the Northern Hemisphere,

could apply here as well: the different structure of the JJA SAM in the two sectors (jet shift, single/double jet see-saw) runs counter to the notion that they share a common dynamical explanation. The situation is however different in the Southern Hemisphere case: the Indian and Pacific sectors are contiguous, and there is no discontinuity in the mean jets or storm tracks like that caused by the American continent in the Northern Hemisphere.

[Figure 11 about here.]

To describe the behaviors of the jets in the two sectors independently from EOF analysis, monthly time-series of the poleward position and speed of the midlatitude jet were computed for both sectors. The 850-hPa wind averaged over the two longitude ranges was used, as it is a better measure of eddy-driven jets than upper-level wind. The zonal wind anomalies regressed on the position and speed indexes are shown on figure 11, together with those related to the SAM. Over the Indian sector, the SAM anomalies are clearly similar to the ones produced by a poleward shift of the jet, with some contribution from jet speed changes at lower latitudes. Over the Pacific sector, the SAM and jet speed anomalies are almost identical. These relations are confirmed by the correlations of the jet indices with the SAM time-series shown on Table 1.

[Table 1 about here.]

Table 1 also shows that variations in the Pacific sector midlatitude jet speed are significantly correlated with latitude shifts of the Indian sector jet, a correlation that the SAM structure is reflecting. No such relation is observed between, for example, the jet latitude in the Indian and Pacific sectors. The jet speed in the two sectors is also correlated; but in the Indian sector jet shifts explain a 50% higher amount of variance and so dominate the SAM signature.

Finally, a relationship between the SAM and the jets similar to the one described in this paper, although not discussed by the authors, is found by Gallego et al. (2005) using different measures of the speed and location of the jet. In another study, limited to interannual variability, Inatsu and Hoskins (2006) used a jet split index defined over the Pacific sector. Their composites and

regression of the zonal wind were very similar to those of figures 3 and 2, including over the Indian sector.

6. Conclusions

The structure and dynamics of the southern annular mode (SAM) have been analyzed for the winter months of June-July-August. It was found that:

1. The spatial structure of height anomalies is annular, with height anomalies of opposing polarities over polar and midlatitude regions. The SAM is associated with a quasi-zonally symmetric dipole of wind anomalies.
2. Composites of total fields show, however, that at different longitudes the SAM corresponds to different kinds of perturbations of the climatological features.

The first sector, covering approximately the Indian ocean, is characterized by a strong mid-latitude jet associated with a wide baroclinic zone and a single storm track. In this sector, opposing polarities of the SAM correspond to a latitudinal shift of the jet and of its associated eddy forcing and maximum baroclinicity.

The second sector, adjacent to the first and covering the western Pacific ocean, is characterized by double jets, and by two distinct maxima of baroclinicity and eddy forcing of the flow. In this sector, the SAM represents opposing changes in the relative amplitude of the two jets, without any latitudinal shift of either jet. This behavior is an example of a dipolar anomaly in zonal wind that does not represent a jet shift.

3. Despite the structural differences, the variability of the two sectors is not independent: low-frequency SAM-related anomalies in the two areas are well correlated, as shown for example by analyses of regional EOFs or of the sectoral variations of the jets characteristics such as speed and latitude.
4. The positive feedback by high-frequency transient eddies plays an important role in the

dynamics of the SAM-related variability. This is not necessarily true however on a more local scale, as eddies influence is exerted downstream of their source regions.

To the extent that the prominence of the SAM is due to the organization of high-frequency eddies in a way that provides a positive feedback, it appears that changes in the background state, with time or through zonal asymmetries, do not modify the basic dynamics of the SAM. Such changes can however modify not only the local amplitude of the SAM (Cash et al. 2005), through changes of forcing or feedback strength (Codron 2005), but also the local relation between the variability and the climatological features. The preferred meridional structure will be probably the one that yields the strongest eddy feedback, given the local mean state (Branstator 1995).

An important consequence is that the annular modes could have a different structure in a different climate: as the climatological features (latitude of the mean jets, relative strength of baroclinic zones) evolve, so could the dominant variability (change in latitude, in variance, or from a jet shift to a see-saw). An example in which the first EOF becomes part of a propagating pattern is given by Son and Lee (2006) in a simplified model. This should be kept in mind for predicting future variability, as well as for reconstructing the past one.

Acknowledgements

The author would like to thank Prof. J. M. Wallace and Dr. Roberta Quadrelli for helpful discussions. The author also thanks Dr. John Fyfe and two anonymous reviewers for their useful comments. Most of this work was conducted during a stay as visiting scientist at the Joint Institute for Study of Atmosphere and Ocean of the University of Washington. The numerical model experiments were conducted at the Institut de Recherches en Informatique Scientifique (IDRIS).

References

- Ambaum, M. H. P., B. J. Hoskins, and D. B. Stephenson, 2001: Arctic oscillation or north Atlantic oscillation? *J. Climate*, **14**, 3495–3507.
- Arblaster, J. M. and G. A. Meehl, 2006: Contributions of external forcings to southern annular mode trends. *J. Climate*, **19**, 2896–2905.
- Bals-Elsholz, T., E. Atallah, L. F. Bosart, T. A. Wasula, M. J. Cempa, and A. R. Lupo, 2001: The wintertime southern hemisphere split jet: Structure variability, and evolution. *J. Climate*, **14**, 4191–4215.
- Blackmon, M. L. and N.-C. Lau, 1980: Regional characteristics of the northern hemisphere wintertime circulation: A comparison of the simulation of a GFDL general circulation model with observations. *J. Atmos. Sci.*, **37**, 497–514.
- Branstator, G., 1995: Organization of storm track anomalies by recurring low-frequency circulation anomalies. *J. Atmos. Sci.*, **52**, 207–226.
- Bretherton, C. S., M. Widmann, V. P. Dymnikov, J. M. Wallace, and I. Blade, 1999: The effective number of spatial degrees of freedom of a time-varying field. *J. Climate*, **12**, 1990–2009.
- Cash, B. A., P. J. Kushner, and G. K. Vallis, 2005: Zonal asymmetries, teleconnections, and annular patterns in a GCM. *J. Atmos. Sci.*, **62**, 207–219.
- Chang, E. K. M., 2005: The role of wave packets in wave-mean flow interactions during southern hemisphere summer. *J. Atmos. Sci.*, **62**, 2467–2483.
- Codron, F., 2005: Relations between annular modes and the mean state: Southern hemisphere summer. *J. Climate*, **18**, 320–330.
- Feldstein, S. and S. Lee, 1998: Is the atmospheric zonal index driven by an eddy feedback? *J. Atmos. Sci.*, **55**, 3077–3086.

- Gallego, D., P. Ribera, R. Garcia-Herrera, E. Hernandez, and L. Gimeno, 2005: A new look for the southern hemisphere jet stream. *Climate Dyn.*, **24**, 607–621.
- Gillett, N. P. and D. W. J. Thompson, 2003: Simulation of recent southern hemisphere climate changes. *Science*, **302**, 273–275.
- Inatsu, M. and B. J. Hoskins, 2004: The zonal asymmetry of the southern hemisphere winter storm track. *J. Climate*, **17**, 4882–4892.
- 2006: The seasonal and wintertime interannual variability of the split jet and the storm-track activity minimum near new zealand. *J. Meteor. Soc. Japan*, **84**, 433–445.
- Kalnay, E. M. and Coauthors, 1996: The NCEP/NCAR Reanalysis Project. *Bull. Am. Meteorol. Soc.*, **77**, 437–471.
- Kushner, P. J., I. M. Held, and T. L. Delworth, 2001: Southern hemisphere atmospheric circulation response to global warming. *J. Climate*, **14**, 2238–2249.
- Lee, S. and H.-K. Kim, 2003: The dynamical relationship between subtropical and eddy-driven jets. *J. Atmos. Sci.*, **60**, 1490–1503.
- L’Heureux, M. L. and D. W. J. Thompson, 2006: Observed relationships between the el niño–southern oscillation and the extratropical zonal-mean circulation. *J. Climate*, **19**, 276–287.
- Lorenz, D. J. and D. L. Hartmann, 2001: Eddy-zonal flow feedback in the southern hemisphere. *J. Atmos. Sci.*, **58**, 3312–3327.
- Quadrelli, R. and J. M. Wallace, 2002: Dependence of the structure of the northern hemisphere annular mode on the polarity of ENSO. *Geophys. Res. Letters*, **29**, 2132.
- Robinson, W. A., 1996: Does eddy feedback sustain variability in the zonal index? *J. Atmos. Sci.*, **53**, 3556–3569.

- 2000: A baroclinic mechanism for the eddy feedback on the zonal index. *J. Atmos. Sci.*, **57**, 415–422.
- Seager, R., N. Harnik, Y. Kushnir, W. Robinson, and J. Miller, 2003: Mechanisms of hemispherically symmetric climate variability. *J. Climate*, **16**, 2960–2978.
- Son, S.-W. and S. Lee, 2005: The response of westerly jets to thermal driving in a primitive equation model. *J. Atmos. Sci.*, **62**, 3741–3757.
- 2006: Preferred modes of variability and their relationship with climate change. *Journal of Climate*, **19**, 2063–2075.
- Thompson, D. W. J. and S. Solomon, 2002: Interpretation of recent southern hemisphere climate change. *Science*, **296**, 895–899.
- Thompson, D. W. J. and J. M. Wallace, 1998: The Arctic Oscillation signature in the wintertime geopotential height and temperature fields. *Geophys. Res. Letters*, **25**, 1297–1300.
- Yang, X. and E. K. M. Chang, 2006: Variability of the southern hemisphere winter split flow—a case of two-way reinforcement between mean flow and eddy anomalies. *J. Atmos. Sci.*, **63**, 634–650.

List of Figures

- 1 Climatological 300-hPa zonal wind for Dec-Jan, Mar-Apr, and Jun-Jul-Aug. Shading levels at 20, 30, 40 m s^{-1} . Thick black lines indicate local maxima (continuous) and minima (dashed) of the wind. 22
- 2 Regressions onto the monthly SAM time-series, for Dec-Jan, Mar-Apr, Jun-Jul-Aug. (top panels) 850-hPa geopotential, contours every 10 m, 0 contour blank, negative contours dashed. (bottom panels) 300-hPa zonal wind (m s^{-1}), the black line indicates the maxima (cont.) and minima (dashed) of the background mean zonal wind. 23
- 3 Composites (JJA) of the 300-hPa zonal wind for the positive (left) and negative (right) phase of the SAM. Contours every 5 m s^{-1} ; bold: 30 m s^{-1} . The dashed meridian in the left panel shows the boundary between the Indian and Pacific sectors (see text). 24
- 4 Composites for the positive (continuous) and negative (dashed) phases of the SAM, for zonally averaged fields over the Indian (left) and Pacific (right) sectors. Top: 300-hPa zonal wind (m s^{-1}); middle: 850-hPa zonal wind (m s^{-1}); bottom: 300-hPa EF [$\text{m}^2\text{s}^{-2} (5^\circ)^{-1}$]. 25
- 5 Composites of the 850-hPa baroclinicity for the positive (cont) and negative (dashed) phase of the SAM, averaged over the Indian sector (top) and the Pacific sector (bottom). Arbitrary units. 26

6	Cross-correlation of the daily SAM time-series with high-frequency eddy forcing of the SAM, averaged over: all longitudes (cont), Indian sector (dashed), Pacific sector (dot-dashed). The dashed horizontal line shows the 95% confidence level. . .	27
7	300-hPa zonally averaged fields regressed upon the standardized SAM time series. Zonal wind (solid, m s^{-1}), and lagged (5-20 days) EF [$\text{m}^2 \text{s}^{-2} (5^\circ)^{-1}$]: high-frequency (dashed) and total (dot-dashed).	28
8	Cross-correlation of high-frequency eddy-forcing of the SAM over the Pacific sector with: daily SAM time series (cont) and SAM 300-hPa zonal wind averaged over the Indian sector (dashed) and over the Pacific sector (dot-dashed). The dashed horizontal line shows the 95% confidence level.	29
9	Composites of the 300-hPa EF, averaged over lags of 10-25 days after positive (cont) and negative (dashed) SAM 300-hPa wind anomalies. Top: Pacific sector EF lagging Indian sector wind. Bottom: Indian sector EF lagging Pacific sector wind. Units: $\text{m}^2\text{s}^{-2} (5^\circ)^{-1}$	30
10	Top: 850-hPa height structure of regional EOF computed over the Indian (left) and Pacific (right) sectors. Contours every 10 m s^{-1} from $\pm 5 \text{ m s}^{-1}$, negative contours dashed. Bottom: 300-hPa zonal wind anomalies, averaged over the Indian (left) and Pacific (right) sectors: regression on the SAM (continuous), as well as on the Indian (dashed) and Pacific (dot-dashed) regional EOFs.	31
11	Zonally-averaged 850 hPa zonal wind anomalies over the Indian (top) and Pacific (bottom) sectors: regression on indexes of the SAM (cont), and of the local jet position (dashed) and jet speed (dot-dashed).	32

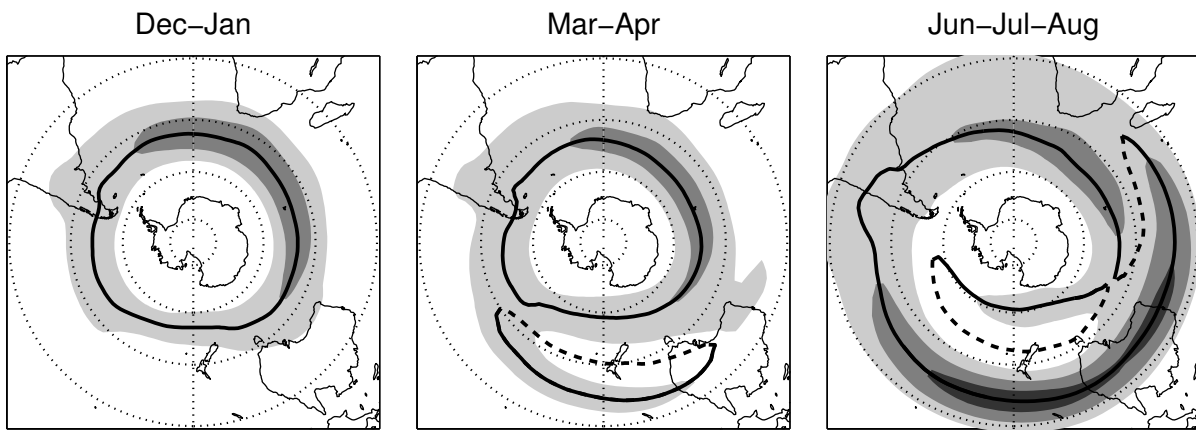


Figure 1: Climatological 300-hPa zonal wind for Dec-Jan, Mar-Apr, and Jun-Jul-Aug. Shading levels at 20, 30, 40 m s^{-1} . Thick black lines indicate local maxima (continuous) and minima (dashed) of the wind.

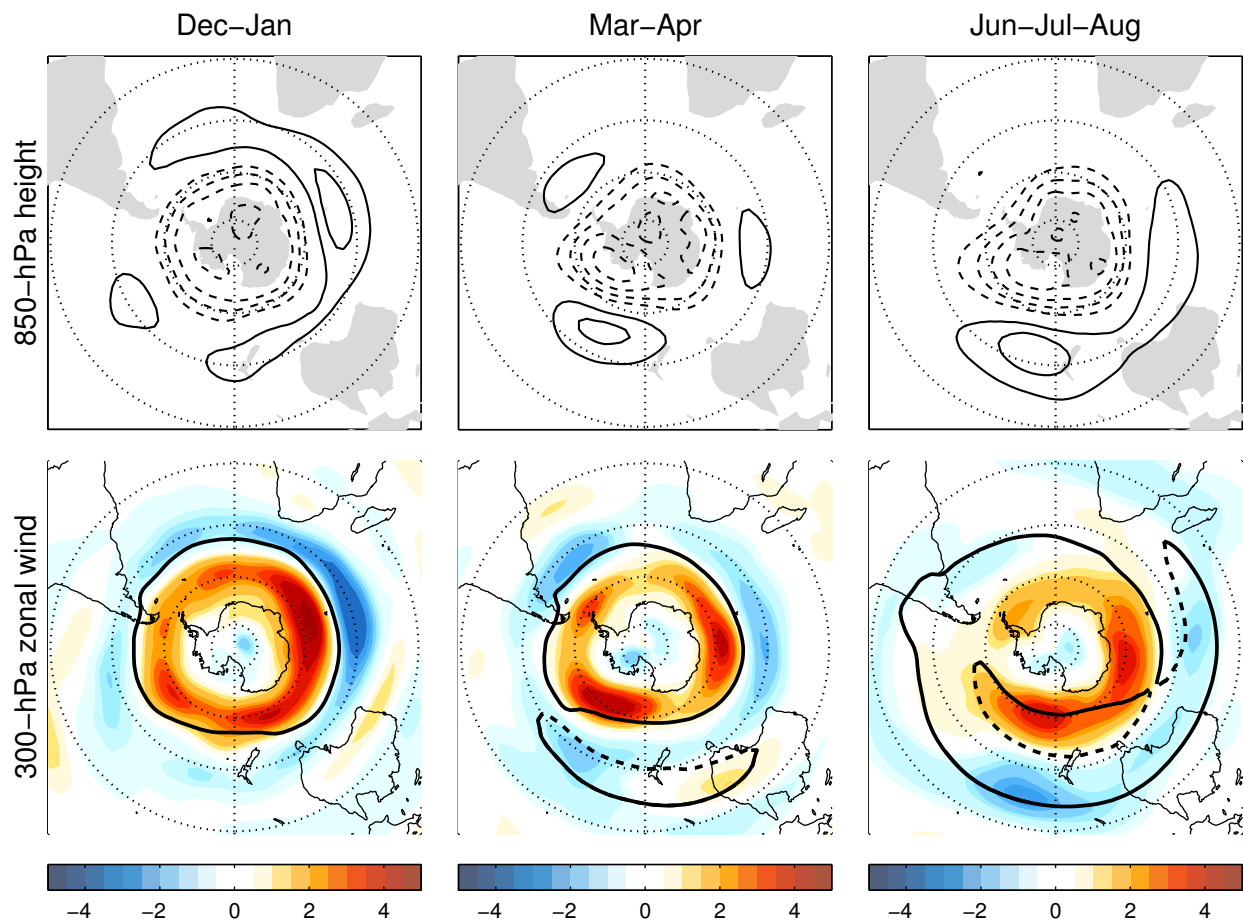


Figure 2: Regressions onto the monthly SAM time-series, for Dec-Jan, Mar-Apr, Jun-Jul-Aug. (top panels) 850-hPa geopotential, contours every 10 m, 0 contour blank, negative contours dashed. (bottom panels) 300-hPa zonal wind (m s^{-1}), the black line indicates the maxima (cont.) and minima (dashed) of the background mean zonal wind.

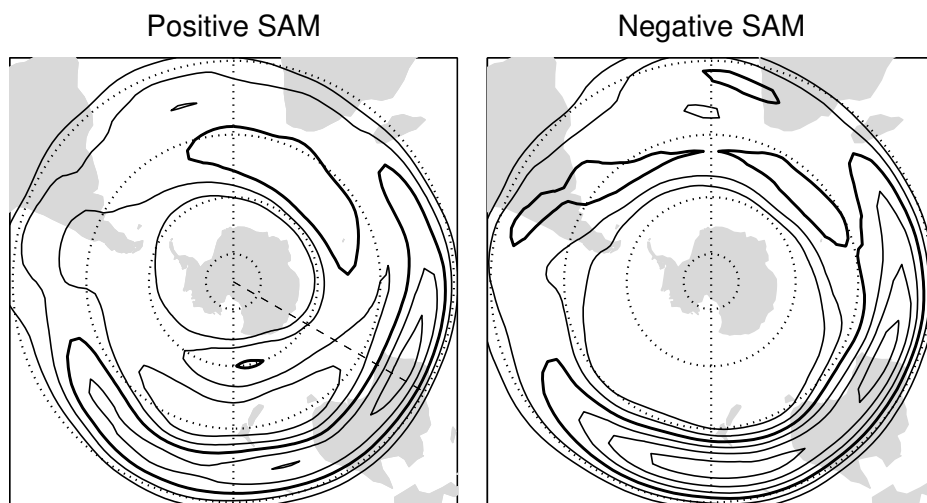


Figure 3: Composites (JJA) of the 300-hPa zonal wind for the positive (left) and negative (right) phase of the SAM. Contours every 5 m s^{-1} ; bold: 30 m s^{-1} . The dashed meridian in the left panel shows the boundary between the Indian and Pacific sectors (see text).

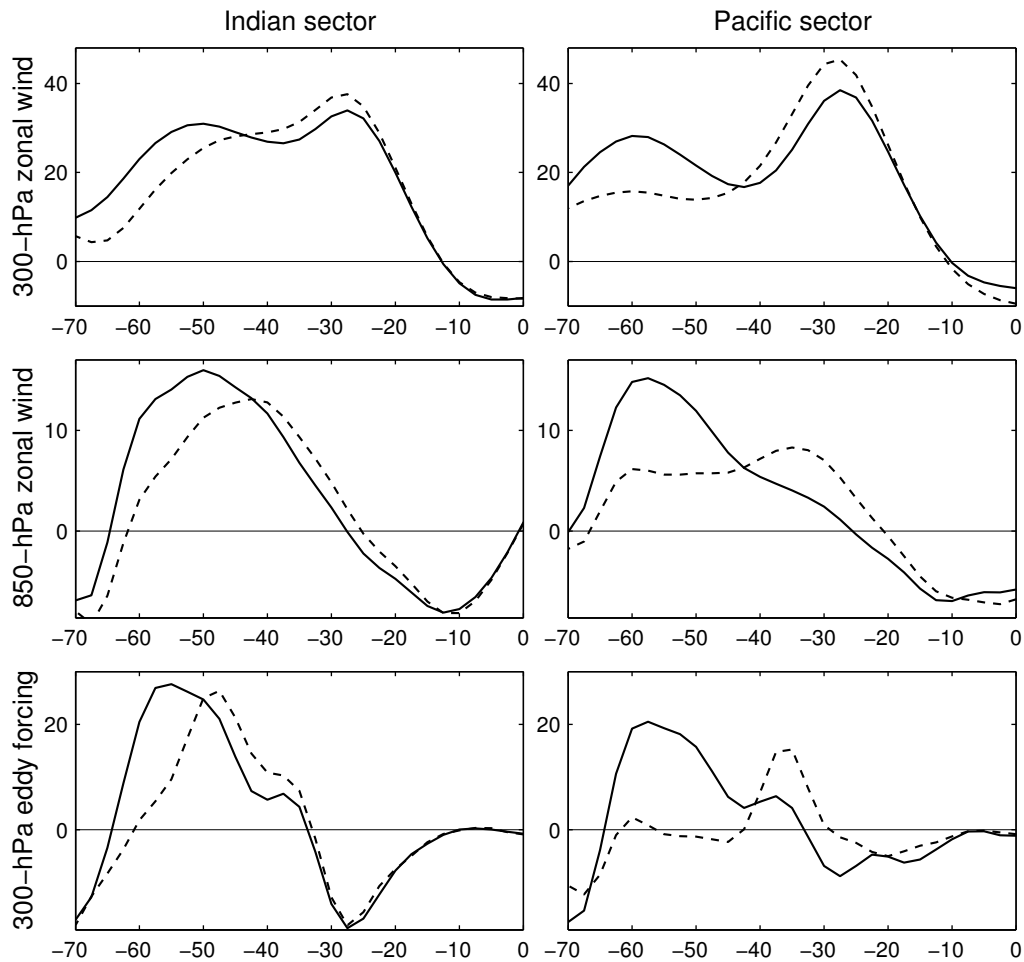


Figure 4: Composites for the positive (continuous) and negative (dashed) phases of the SAM, for zonally averaged fields over the Indian (left) and Pacific (right) sectors. Top: 300-hPa zonal wind (m s^{-1}); middle: 850-hPa zonal wind (m s^{-1}); bottom: 300-hPa EF [m^2s^{-2} (5°) $^{-1}$].

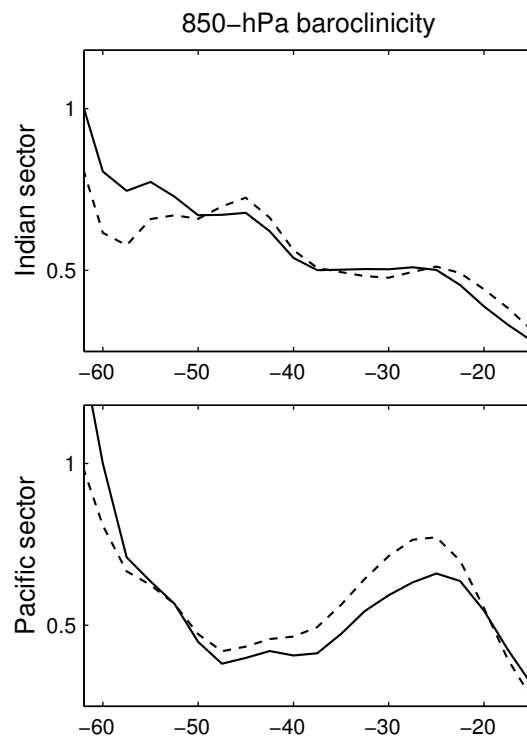


Figure 5: Composites of the 850-hPa baroclinicity for the positive (cont) and negative (dashed) phase of the SAM, averaged over the Indian sector (top) and the Pacific sector (bottom). Arbitrary units.

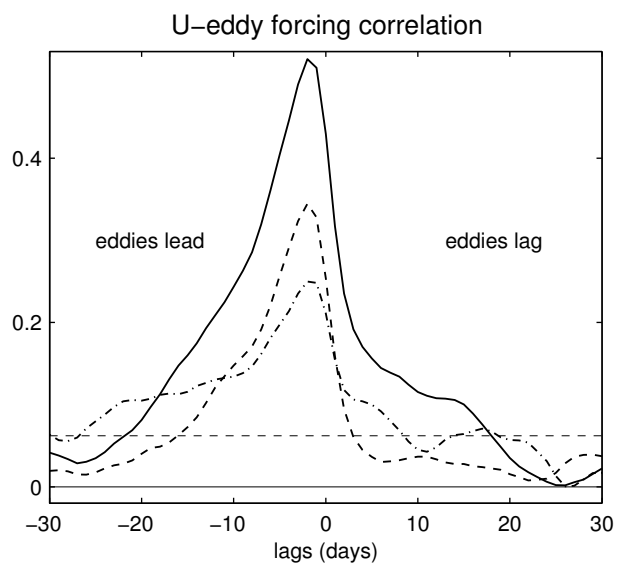


Figure 6: Cross-correlation of the daily SAM time-series with high-frequency eddy forcing of the SAM, averaged over: all longitudes (cont), Indian sector (dashed), Pacific sector (dot-dashed). The dashed horizontal line shows the 95% confidence level.

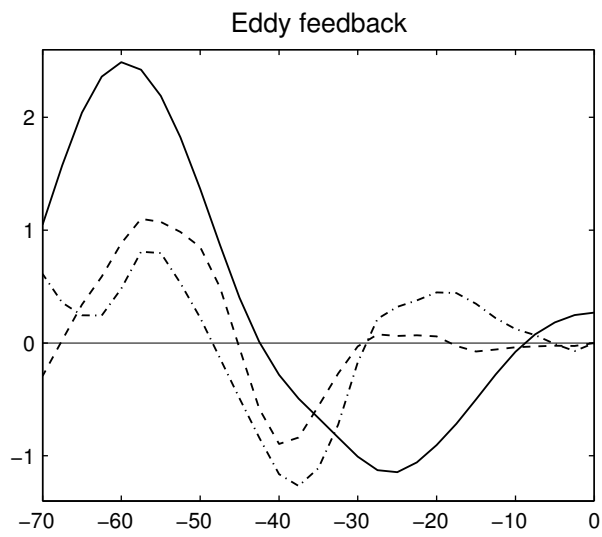


Figure 7: 300-hPa zonally averaged fields regressed upon the standardized SAM time series. Zonal wind (solid, m s^{-1}), and lagged (5-20 days) EF [$\text{m}^2 \text{s}^{-2} (5^\circ)^{-1}$]: high-frequency (dashed) and total (dot-dashed).

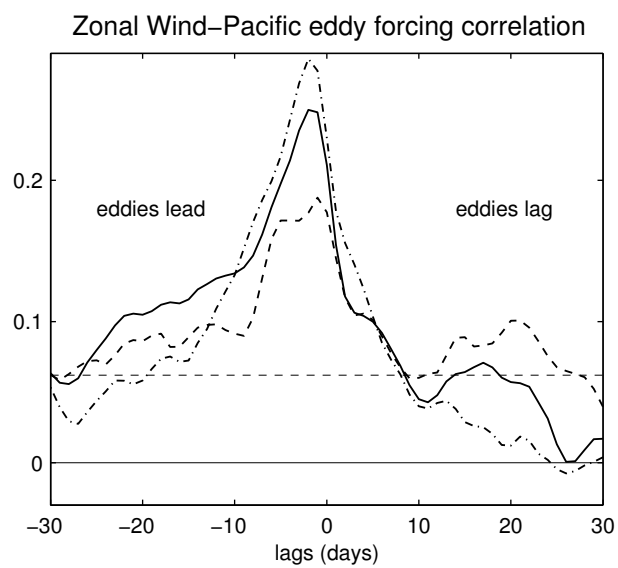


Figure 8: Cross-correlation of high-frequency eddy-forcing of the SAM over the Pacific sector with: daily SAM time series (cont) and SAM 300-hPa zonal wind averaged over the Indian sector (dashed) and over the Pacific sector (dot-dashed). The dashed horizontal line shows the 95% confidence level.

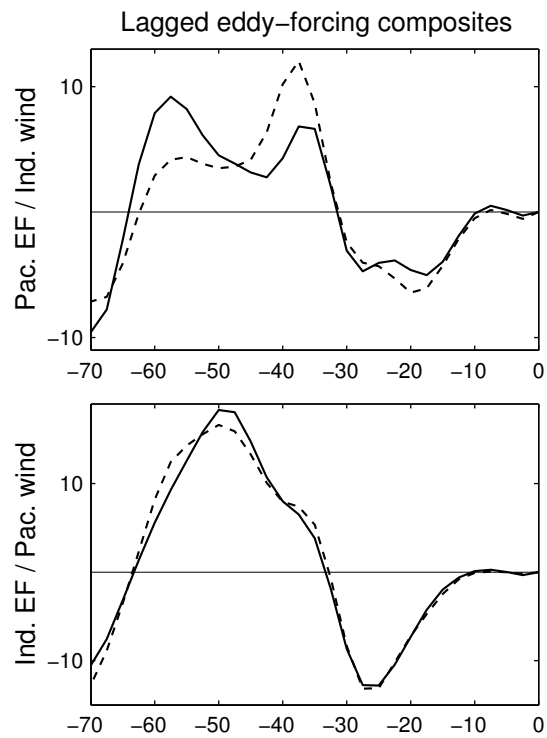


Figure 9: Composites of the 300-hPa EF, averaged over lags of 10-25 days after positive (cont) and negative (dashed) SAM 300-hPa wind anomalies. Top: Pacific sector EF lagging Indian sector wind. Bottom: Indian sector EF lagging Pacific sector wind. Units: $\text{m}^2\text{s}^{-2} (5^\circ)^{-1}$

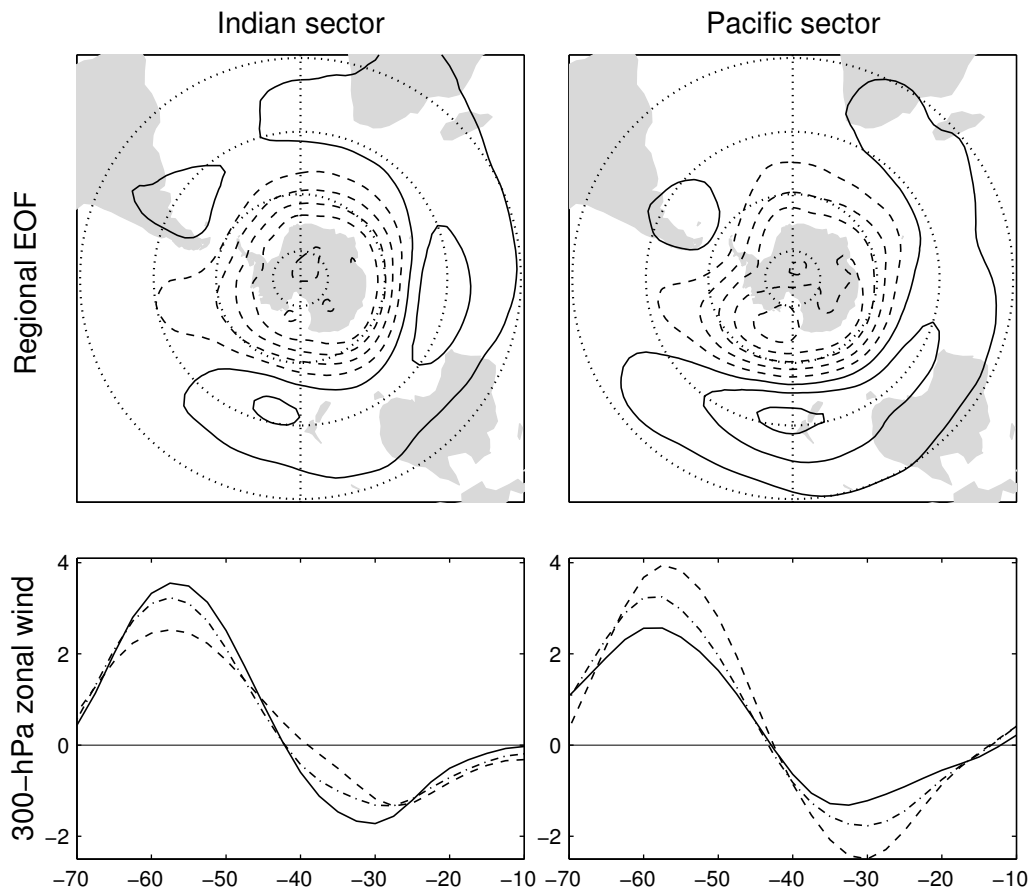


Figure 10: Top: 850-hPa height structure of regional EOF computed over the Indian (left) and Pacific (right) sectors. Contours every 10 m s^{-1} from $\pm 5 \text{ m s}^{-1}$, negative contours dashed. Bottom: 300-hPa zonal wind anomalies, averaged over the Indian (left) and Pacific (right) sectors: regression on the SAM (continuous), as well as on the Indian (dashed) and Pacific (dot-dashed) regional EOFs.

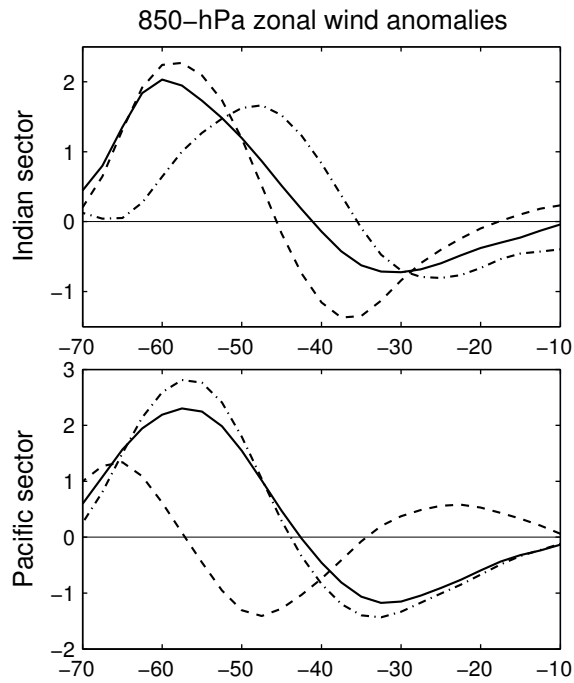


Figure 11: Zonally-averaged 850 hPa zonal wind anomalies over the Indian (top) and Pacific (bottom) sectors: regression on indexes of the SAM (cont), and of the local jet position (dashed) and jet speed (dot-dashed).

List of Tables

- 1 Jet position and speed indices statistics. Top rows: correlations with monthly time-series of the SAM. Jet position index is positive when the jet is displaced poleward. Correlations in bold are significant at the 99% level, others are insignificant even at 95%. Bottom rows: percentages of the global (Southern Hemisphere) and local (respective sector) area-weighted variance of the 850-hPa geopotential explained by the indices. 34

Table 1: Jet position and speed indices statistics. Top rows: correlations with monthly time-series of the SAM. Jet position index is positive when the jet is displaced poleward. Correlations in bold are significant at the 99% level, others are insignificant even at 95%. Bottom rows: percentages of the global (Southern Hemisphere) and local (respective sector) area-weighted variance of the 850-hPa geopotential explained by the indices.

	Ind. position	Ind. speed	Pac. position	Pac. speed
Correlation with SAM	.54	.43	-.08	.80
Correlation with Pac. speed	.35	.40	-.03	-
Correlation with Pac. position	.14	-.09	-	-
Explained var. (local)	23%	14%	5.5%	35%
Explained var. (global)	11%	6%	2.7%	20%